Poly(A)-specific ribonuclease deficiency impacts telomere biology causing dyskeratosis congenita

Hemanth Tummala, Amanda Walne, Laura Collopy, Shirleny Cardoso, Josu de la Fuente, Sarah Lawson, James Powell, Nicola Cooper, Alison Foster, Shehla Mohammed, Vincent Plagnol, Thomas Vulliamy, Inderjeet Dokal

Supplemental Material consists of 1 table and 5 figures.

Supplemental Table 1: Primer sequences for genes assessed by qPCR.

Gene	Forward Sequence	Reverse Sequence
ACTB	GACGACATGGAGAAAATCTG	ATGATCTGGGTCATCTTCTC
TERC	TCTAACCCTAACTGAGAAGG	GTTTGCTCTAGAATGAACGG
DKC1	CTGGAGTCATGAGTGAAAAG	CTCATCCTTGTGGTTATCATAC
TERF1	GGATACAAGAAAAAGGTCTCAC	CAGGTATTCTGCTTTCAGTG
RTEL1	TCCCAAAGATTATTTACGCC	TCTGTAGATGGTTACTCTCTTG
NOP10	TACGCTGAAGAAATTTGACC	GTGTCGAGAGTATTTGTCATC
CTC1	GCTGTTACTTTTAGGGACAC	GAAAGGTCCAGGTCTATGAG
TINF2	CAGGAACTTGAACAAGAGTATG	GAAGAGGTGATAGAGACTCC
TEN1	AACATTTGGCAGGTTGTG	AACTTGGTACAGACAAGAAC
OBFC1	TTACTATAAAGTGGACGACCC	TCTTTGGCTTTTTCACTCAG
NHP2	AGGAGAAAAAGGGATCATGG	GAGGGGATATAGACATAGGG

All sets were obtained from Sigma from their KiCqStart range.

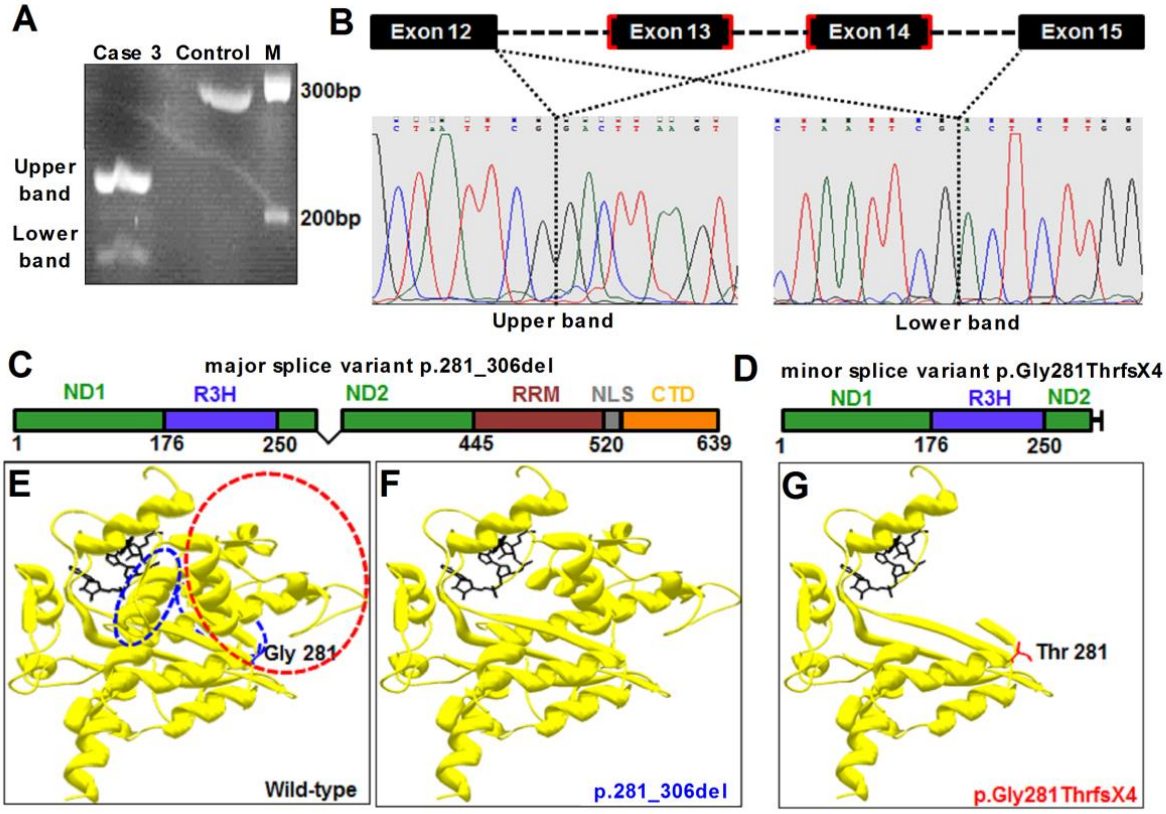

Supplemental Figure 1: Characterization of the *PARN* mutation identified in case 3. (A) RTPCR analysis of blood cDNA from case 3 revealed two distinct abnormal bands (upper and lower) on an agarose gel when compared to an unrelated control ('M' refers to a 100bp DNA ladder marker). (B) Sanger sequencing of the major upper band revealed skipping of exon 13, while the minor lower band revealed the skipping of both exons 13 and 14. (C and D) Schematic representations of the resultant protein of the major splice variant (C) and the minor splice variant (D). (E) The crystal structure of the wild type PARN ND2 domain (PDB id: 2A1S) (13) shows the deleted regions marked in dotted blue for major splice variant and dotted red for minor splice variant. (F and G) In silico analysis of the resulting structures show loss of an α helix and a β sheet in PARN ND2 crystal structure for the major splice variant (F) and premature truncation resulting in loss of the RRM and CTD for the minor splice variant due to a frame shift caused by the aberrant splicing (G).

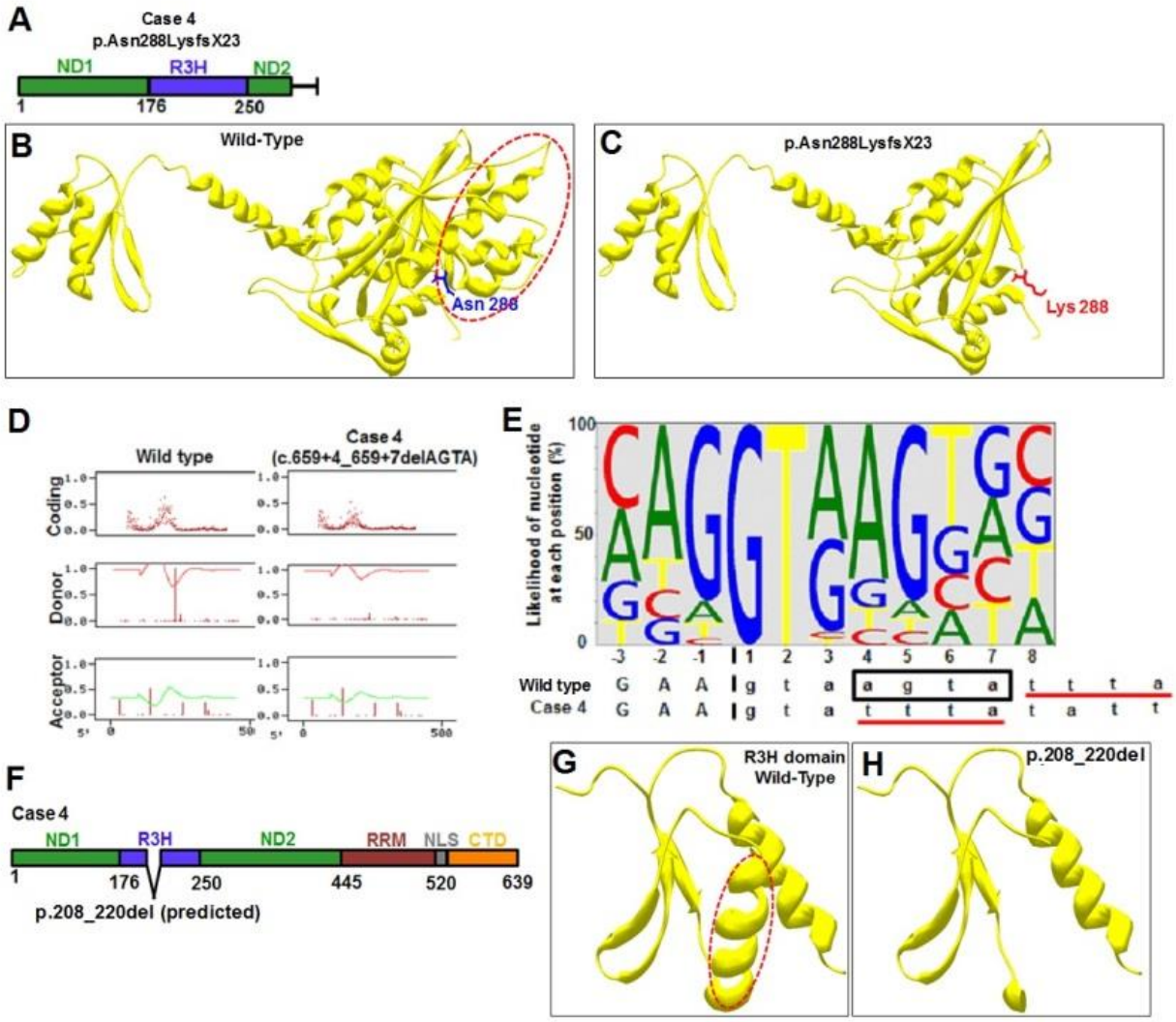

Supplemental Figure 2: Characterization of *PARN* mutations identified in case 4. (A) The c.863dupA frameshift mutation in case 4 results in loss of the ND2, RRM and CTD in PARN. (B and C) In silico analysis of the PARN crystal structure (PDB id: 2A1R). (B)The dotted red ellipse shown on the wild type indicates the position of the structural deletion and (C) the resultant truncated product of p.Asn288LysfsX23. (D and E) The c.659+4_659+7delAGTA mutation is predicted to cause the loss of the donor splice site resulting in the skipping of exon 9. (D) NetGene 2 prediction (www.cbs.dtu.dk/services/NetGene2) shows the loss of the donor splice site when a 500bp fragment containing the mutation is compared to wild type, as indicated by the loss of the tall vertical red line present in the wild type donor panel. (E) 5' consensus donor sequence logo (from http://www.uni-duesseldorf.de/rna/html/background) is shown above the normal sequence of the *PARN* exon/intron 9 junction, as well as the sequence seen in case 4. The black box identifies the deleted nucleotides (F) Schematic diagram of the predicted spliced mutant product (p.208_220del) showing a partial loss of the R3H domain in the PARN protein. (G) A structural view of wild type PARN R3H domain. The deleted region is indicated (dotted red). (H) The predicted loss of exon 9 would result in the loss of an α helix in the R3H domain of PARN.

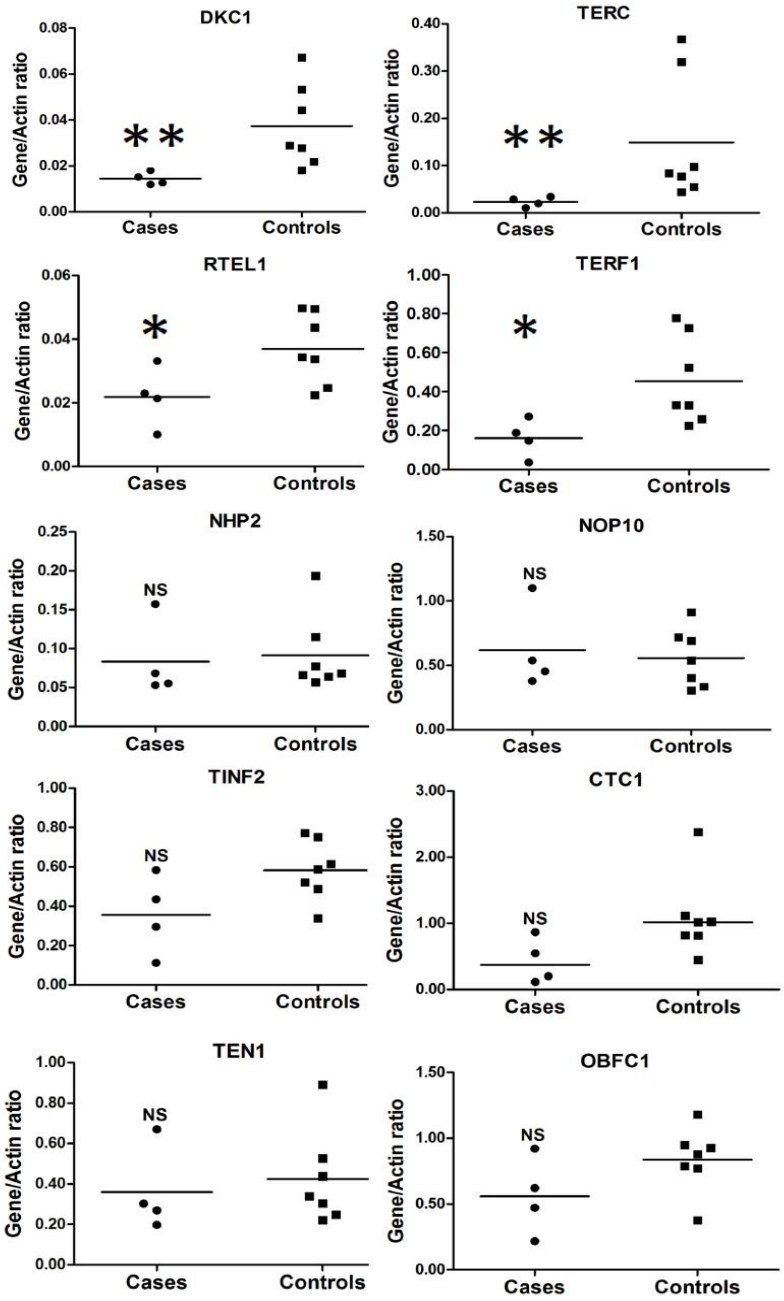

Supplemental Figure 3: The effect of PARN deficiency on genes involved in telomere biology

qPCR analysis on total cDNA prepared from peripheral blood from cases with PARN mutations and controls. Equal amounts of cDNA, prepared using random hexamers were used in qRT–PCR reactions using primers specific to telomere maintenance genes, seven of which (*DKC1*, *TERC*, *RTEL1*, *NHP2*, *NOP10*, *CTC1* and *TINF2)* are found to be mutated in DC. One sample from case 1 and case 2 and two independent samples from case 3 were available for analysis, as well as single samples from seven controls. Data is shown as a relative expression of gene transcript as a ratio to β-actin and normalized to a healthy male control. * $p<0.05$, ** $p<0.01$, Mann Whitney U test. Bar represents median relative expression ratio.

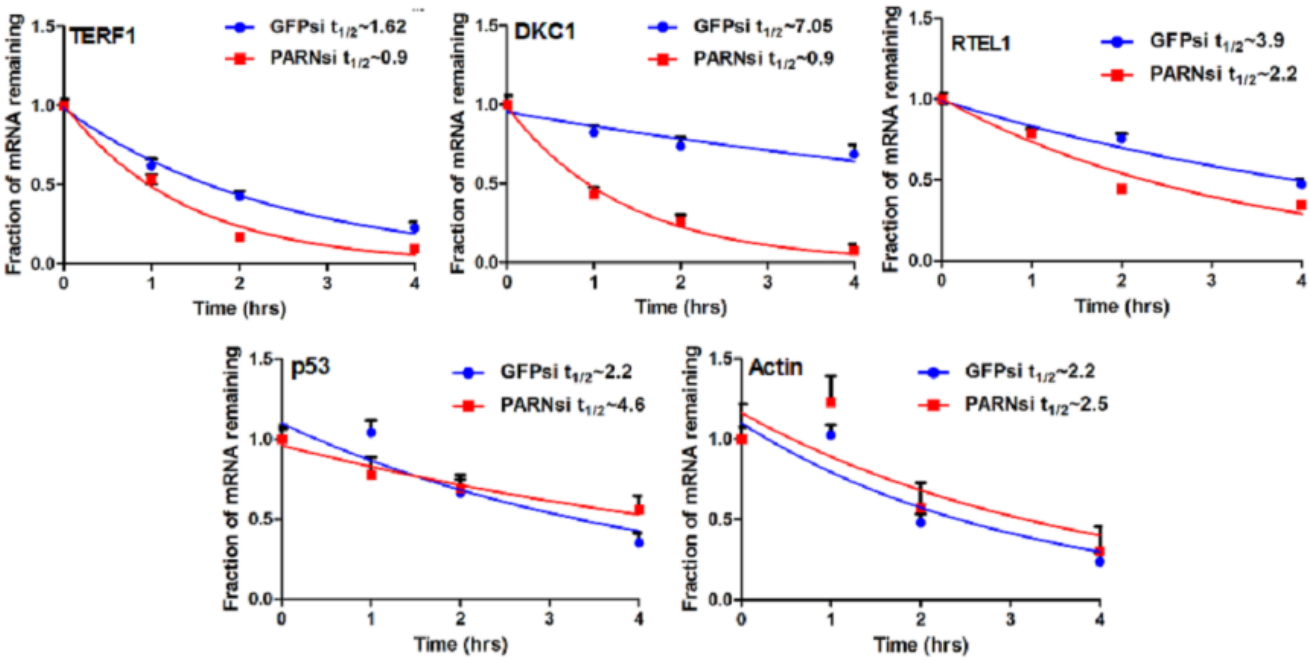

Supplemental Figure 4: PARN deficiency alters telomeric mRNA transcript stability
mRNAs' stability were determined following Actinomycin-D treatment. mRNA abundance at each time point was assessed by qPCR. β-actin and p53 are used as positive controls for determining PARN specific effects on mRNA regulation as described previously (12, 25). For clarity only the positive SEM is shown. The results are the average of triplicates from two independent experiments.

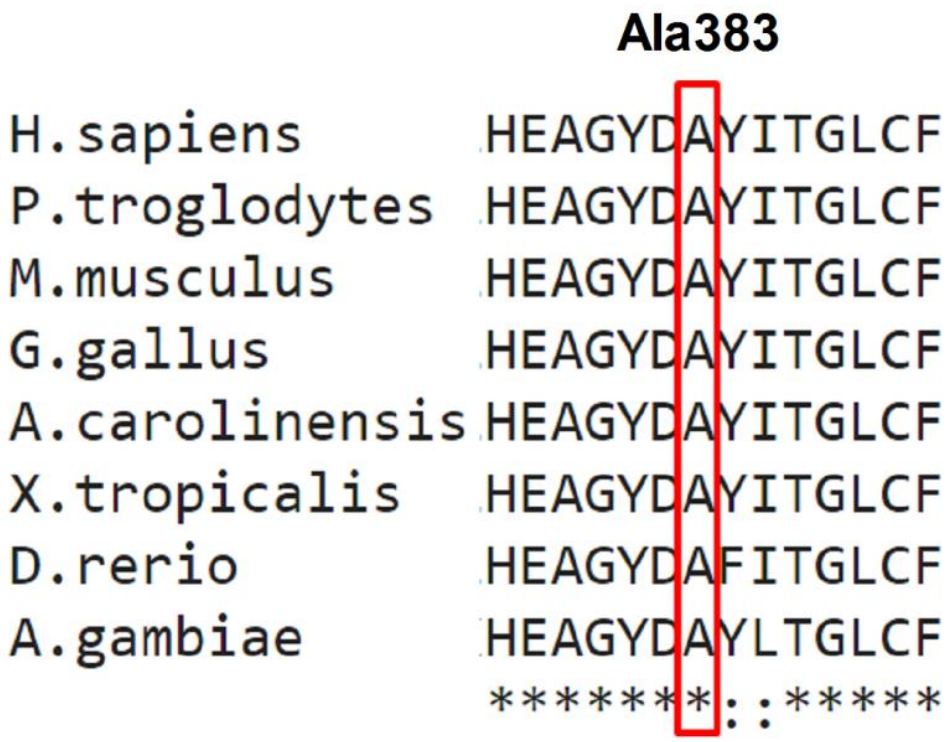

Supplemental Figure 5: Conservation of amino acid (Ala383) in PARN which is mutated in cases of family 1.

Blocks of amino acid alignment were generated with ClustalW and show the degree of conservation of the altered alanine residue at position 383 to valine. Asterisks indicate positions that have a single fully conserved residue; colons indicate conservation between groups of strongly similar properties. Accession numbers: H. sapiens NP_002573; P. troglodytes XP_510832; M. musculus NP_083037; G. gallus NP_001025800; A. carolinensis XP_003228705; X. tropicalis NP_001184102; D. rerio NP_957382; A. gambiae XP_308433.